Amyloid-β Aggregation: Selective Inhibition of Aggregation in Mixtures of Amyloid with Different Chain Lengths

Seth W. Snyder, Uri S. Ladror, Warren S. Wade, Gary T. Wang, Leo W. Barrett, Edmund D. Matayoshi, Helen Jan Huffaker, Grant A. Krafft, and Thomas F. Holzman
Drug Design and Delivery, Pharmaceutical Products Division, Abbott Laboratories, Abbott Park, Illinois

ABSTRACT One of the clinical manifestations of Alzheimer's disease is the deposition of the 39–43 residue amyloid-β (Aβ) peptide in aggregated fibrils in senile plaques. Characterization of the aggregation behavior of Aβ is one of the critical issues in understanding the role of Aβ in the disease process. Using solution hydrodynamics, Aβ was observed to form three types of species in phosphate-buffered saline: insoluble aggregates with sedimentation coefficients of ~50,000 S and molecular masses of $\sim 10^9$ Da, "soluble aggregates" with sedimentation coefficients of ~30 S and masses of $\sim 10^6$ Da, and monomer. When starting from monomer, the aggregation kinetics of Aβ 1–40 (Aβ40) and Aβ 1–42 (Aβ42), alone and in combination, reveal large differences in the tendency of these peptides to aggregate as a function of pH and other solution conditions. At pH 4.1 and 7.0–7.4, aggregation is significantly slower than at pH 5 and 6. Under all conditions, aggregation of the longer Aβ42 was more rapid than Aβ40. Oxidation of Met-35 to the sulfoxide in Aβ40 enhances the aggregation rate over that of the nonoxidized peptide. Aggregation was found to be dependent upon temperature and to be strongly dependent on peptide concentration and ionic strength, indicating that aggregation is driven by a hydrophobic effect. When Aβ40 and Aβ42 are mixed together, Aβ40 retards the aggregation of Aβ42 in a concentration-dependent manner. Shorter fragments have a decreasing ability to interfere with Aβ42 aggregation. Conversely, the rate of aggregation of Aβ40 can be significantly enhanced by seeding slow aggregating solutions with preformed aggregates of Aβ42. Taken together, the inhibition of Aβ42 aggregation by Aβ40, the seeding of Aβ40 aggregation by Aβ42 aggregates, and the chemical oxidation of Aβ40 suggest that the relative abundance and rates of production of different-length Aβ and its exposure to radical damage may be factors in the accumulation of Aβ in plaques in vivo.

INTRODUCTION

The formation of extracellular deposits of neuritic (senile) plaques is one hallmark of Alzheimer's disease (AD). The major component of these plaques is amyloid-β (Aβ), a 39–43-residue peptide (Glenner and Wong, 1984; Kang et al., 1987). The sequence of Aβ 1–42 is: DAEFR^{5}HDSGY^{10}EVHHQ^{15}KLVFF^{20}AEDVG^{25}SNKGA^{30}-IILGLM^{35}VGGVV^{40}IA. Aβ is derived by proteolytic cleavage of the transmembrane region of the 110–135-kDa amyloid precursor protein (βPP; Goldgaber et al., 1987; Kang et al., 1987; Kitaguchi et al., 1988; Ponte et al., 1988; Tanzi et al., 1988). Evidence suggests that accumulation of Aβ and formation of the neuritic plaques may play a pathological role in the disease (Kowall et al., 1991; Yankner, 1992; Krafft, 1993; Selkoe, 1993). Reports from in vitro toxicity studies have suggested that soluble Aβ is nontoxic, whereas aggregated Aβ is toxic (Pike et al., 1991; Burdick et al., 1992; Mattson and Rydel, 1992; Yankner, 1992; Pike et al., 1993; Giordano et al. 1994). Soluble Aβ is present as a normal extracellular product in a variety of cell lines (Haass et al., 1992) and is found at comparable levels in the cerebrospinal fluid of age-matched AD and normal patients (Seubert et al., 1992; Shoji et al., 1992).

Aβ forms antiparallel β-pleated sheets that aggregate into amyloid fibrils that exhibit positive Congo Red staining (Glenner, 1980; Kirschner et al., 1987; Turnell and Finch, 1992). A number of techniques, including circular dichroism, nuclear magnetic resonance (NMR), and infrared, have been employed to characterize the secondary molecular structure and conformation of Aβ (Masters et al., 1985; Halvserson et al., 1990; Fraser et al., 1991; Hilbich et al., 1991; Spencer et al., 1991; Barrow et al., 1992; Fraser et al., 1992; Lansbury, 1992; Zagorski and Barrow, 1992). The degree of β-sheet character and transitions to either α-helix or random coil have proven to be strongly dependent upon the solution characteristics. Observations of molecular structural variability have been attributed to a number of physical and environmental characteristics, including the length of the Aβ fragment, peptide concentration, age of the sample, presence of organic solvents, temperature, solution pH, and ionic strength (Fraser et al., 1991; Hilbich et al., 1991; Barrow et al., 1992; Fraser et al., 1992; Zagorski and Barrow, 1992; Otvos et al., 1993).

The fibrillar structure of Aβ aggregates has been investigated with electron microscopy, x-ray diffraction, and light scattering (Gorevic et al., 1986; Kirschner et al., 1987; Halvserson et al., 1990; Caputo et al., 1992; Fraser et al., 1992; Caputo et al., 1993; Inouye et al., 1993). Reports indicate that the fibrils formed from purified Aβ are relatively straight with a diameter of 5 nm and periodic twists (Fraser et al., 1992). These structures have generally correlated with the structures observed of fibrils in senile plaques from AD brains (Kirschner et al., 1986).

It is reasonable to assume, a priori, that the ability of Aβ to accumulate in senile plaques in vivo strongly depends on

Received for publication 15 April 1994 and in final form 22 June 1994.
Address reprint requests to Dr. Thomas F. Holzman, D-46Y, AP-10, Protein Biochemistry, Pharmaceutical Discovery Research, Abbott Laboratories, 1 Abbott Park Road, Abbott Park, IL 60064–3500. Tel.: 708-937-2104; Fax: 708-938-2258; E-mail: holzman@abbott.com.

0006-3495/94/09/1216/13 $2.00

at least two factors, local concentration and the kinetics of aggregation. If Aβ aggregation is slow in vivo, it may be cleared by proteolytic degradation before its deposition (Hyman et al., 1993; Ladror et al., 1993, 1994, Suzuki et al., 1994). Conversely, if the seeded aggregate structure becomes resistant to proteolysis in vivo more rapidly than it is degraded, the seeds will grow into larger aggregates and senile plaques could form. There have been several investigations of the kinetics of Aβ aggregation (Tomski and Murphy, 1992; Jarrett and Lansbury, 1993; Jarrett et al., 1993; Shen et al., 1993; Snyder et al., 1993a,c). Most of the work has focused on kinetic events that occur over the course of hours to days. In general, conditions that favor β-sheet structure also enhance aggregation rates (Tomski and Murphy, 1992; Jarrett and Lansbury, 1993; Jarrett et al., 1993).

Observations regarding aggregate size and structure, as well as the kinetics of aggregation, have exhibited considerable variability as a result of different peptide-handling procedures and techniques employed to monitor and characterize aggregation behavior (Knauer et al., 1992; Simmons et al., 1993, 1994; Snyder et al., 1993b,c). One cause of the discrepancy regarding Aβ aggregation and toxicity is the method of dissolving and handling Aβ. Typically, experiments have been performed by directly transferring Aβ from a lyophilized solid to the solution conditions employed for aggregation, structure, or toxicity studies (Hilbich et al., 1991; Burdick et al., 1992; Tomski and Murphy, 1992). There has been no consideration for the effect of high local Aβ concentrations on aggregation behavior during the nonhomogeneous solvation process. At high concentrations of synthetic Aβ, variations in acid or water content may accentuate the nonhomogeneous distribution during mixing of the lyophilized solid. Furthermore, little regard has been shown for potential aggregation in intermediate Aβ solutions used between concentrated stock solutions and dilute final solutions. At intermediate dilutions, Aβ remains relatively concentrated, whereas organic solvent concentrations are reduced, which can lead to rapid aggregation. Besides variations in Aβ solvation, differences exist in the techniques employed to characterize the degree of Aβ aggregation. The sensitivity of dye staining such as thioflavine T to either small soluble aggregates or rapidly formed aggregates with little structural integrity remains unclear (LeVine, 1993). The effect of SDS on the stability of Aβ aggregates precludes gel electrophoresis as a reliable quantitative technique for assessing aggregation. Finally, a variety of studies have been conducted with the implicit presumption that all aggregated Aβ is removed by centrifugation at 10,000–100,000 × g (Burdick et al., 1992; Waite et al., 1992; LeVine, 1993).

A paradigm for studying amyloid aggregation depends upon the ability to define an initial solute physical state, to monitor the transition process from an initial state to a final state, and to define the final (equilibrium) state (Snyder et al., 1993a-c). Rates of aggregation, in vivo, that are so sluggish that they preclude accumulation in competition with proteolysis cannot be considered relevant (Hyman et al., 1993; Ladror et al., 1993, 1994; Suzuki et al., 1994). Therefore, we have undertaken a systematic investigation of the propensity of Aβ to aggregate under conditions in which peptide accumulation would be expected to compete with physiological degradation. In this work, we describe the aggregation of Aβ from a hydrodynamically defined, monomeric starting state to a fibrillar final state. We find that kinetics are strongly dependent on fragment length, pH, concentration, seeding, and ionic strength. We further demonstrate that aggregation kinetics of the more hydrophobic Aβ 1–42 (Aβ42) can be selectively inhibited, in a specific and dose-dependent fashion, by the more soluble Aβ 1–40 (Aβ40). In addition, we demonstrate that oxidation of the single Met-35 residue in Aβ40 to the more polar sulfoxide form, (Aβ40 M[O]), enhances aggregation rate. From the dependence of aggregation kinetics on relative concentrations of Aβ40 and Aβ42, we suggest that selectivity of cleavage in the carboxy terminus of APP and the potential for Met-35 oxidation may be factors in the accumulation of Aβ in senile plaques.

MATERIALS AND METHODS

Peptide synthesis and purification

The methods used for peptide synthesis and the characterization of the resulting peptides are briefly summarized. Solid-phase peptide synthesis was carried out on an Applied Biosystems (Foster City, CA) Model 430A peptide synthesizer operating with Fmoc chemistry based on dicyclohexylcarbodiimide-catalyzed formation of 1-hydroxytriazole ester in *N*-methylpyrolidone (NMP) and dichloromethane (DCM) co-solvent. Fmoc removal (deprotection of amino groups) was achieved with 20% piperidine in NMP. The side chain protecting groups were as follows: Ser and Tyr, O-t-Bu; Asn and Gln, C(O)-NH-Trityl; Asp and Glu, CO_2-t-Bu; His, Trityl; Lys, Boc-NH; Arg, N^G-(2,2,5,7,8-pentamethylchroman-6-sulfonyl). All natural amino acids were purchased from ABI. Fmoc-Met oxide for the synthesis of Aβ40 Met-35[O] (Aβ40 M[O]) was either prepared by oxidation of Fmoc-Met with *m*-chloroperbenzoic acid in DCM or purchased from Bachem (Torrance, CA). ABI *p*-hydroxymethylphenoxymethyl resin with a substitution level of 0.85 mmol/g was used for synthesis. A standard double-loading cycle involving coupling in the presence of *p*-dimethylaminopyridine was used to load the first residue on to the resin. Coupling of all subsequent residues was achieved using standard double-coupling cycles with acetyl capping supplied with the instrument. In our hands syntheses performed as described above exhibited a typical coupling efficiency of 99.6% by ninhydrin analysis.

Upon completion of a synthesis, the peptide resin was treated with a mixture of trifluoroacetic acid (TFA, 93%) and a scavenger cocktail (7%) composed of ethylene dithiol, anisole, and ethylmethyl sulfide in a 1:3:3 ratio for 3–4 h. The cleavage reagents were typically used at 20 ml/g of peptide resin. At the end of cleavage the resin was removed by filtration and the solvents were evaporated. The crude peptide was precipitated with diethyl ether and collected. The amount of crude peptide obtained typically corresponded to ~95% of the expected theoretical yield based on the amount of resin used. The crude peptides were routinely analyzed by reversed phase high-performance liquid chromatography (RP-HPLC) and mass spectrometry. Preparative peptide isolations were performed using a 40-mm C8 column (300 Å, 12 μm) at 45 ml/min. Before elution of each peptide the acetonitrile (ACN) gradient was reduced to 0.6% ACN/min to broaden the eluting peak. Only the center of each peak was collected (~85% of peak area). The pooled HPLC fractions were lyophilized and the products further analyzed by analytical RP-HPLC and electrospray ionization mass spectrometry (ESI-MS) to establish purity. Typical purity values were >95% for Aβ40 and >85% for Aβ42.

Sample preparation

Aβ samples were stored in lyophilized form at room temperature, and were dissolved in stock solutions in either dimethyl sulfoxide (DMSO), 30%

ACN with 0.1% TFA (ACN/TFA), hexafluoroisopropanol (HFIP), or H_2O at concentrations up to 30 mg/ml (~6.5 mM). Dilution was accomplished in one step from the concentrated stocks into the final buffer, avoiding intermediate solutions with high Aβ concentrations between the starting stock and final solutions. Samples were dissolved in either of two buffers: phosphate-buffered saline (PBS) composed of phosphate (10–50 mM), NaCl (0–500 mM, pH 7.40); or a wide-range pH buffer composed of HOAc (20 mM), MES (20 mM), Tris (20 mM), glycine (20 mM), NaCl (150 mM, pH 3–9).

Analytical ultracentrifugation measurements

Sedimentation equilibrium and velocity measurements were performed on a Beckman (Palo Alto, CA) XL-A analytical ultracentrifuge with an An60Ti rotor (Holzman and Snyder, 1994). Most experiments were carried out at 23.0°C. Equilibrium runs were performed on 110-μl samples over the rotor velocity range 3000–60,000 rpm. Samples were centrifuged for at least 20 h to reach equilibrium and signals were averaged 4 to 16 times. Data were analyzed for solute molecular weights as recently described (Holzman and Snyder, 1994). Velocity runs were performed on 300–450-μl samples over the rotor velocity range of 1000–30,000 rpm. Analysis of velocity data for sedimentation and diffusion coefficients for single solutes and multiple, noninteracting solutes were based on a form of Faxén's two-component solution to the Lamm equation, as described by Fujita (1962). The useful expression is:

$$c = \left(\frac{c_0 e^{-\tau}}{2}\right)\left[1 - \Phi\left(\frac{1 - (xe^{-\tau})^{1/2}}{[\epsilon(1 - e^{-\tau})]^{1/2}}\right)\right] \quad (1)$$

where $x = (r/r_0)^2$, $\tau = 2s\omega^2 t$, $\epsilon = 2D/s(\omega r_0)^2$, Φ is the error function of the term enclosed in brackets, r is the radial position, r_0 is the radial position of the meniscus, ω is the radial rotor velocity, t is the time, and s and D are the sedimentation and diffusion coefficients, respectively. The sedimentation coefficient is reported in Svedbergs (S, 10^{-13} s^{-1}) and the diffusion coefficient in Ficks (10^7 cm^2/s). Under suitable conditions (Fujita, 1962), Eq. 1 can be used to approximate the profile of a sedimenting boundary (Holzman and Snyder, 1994). For heterogeneous samples or samples with multiple sedimenting components with different values of s and D, the sedimenting boundary can be represented as a linear sum of terms identical to Eq. 1, where each term represents a component with specific value of s and D (Holzman and Snyder, 1994). A sample with multiple sedimenting components of similar hydrodynamic properties can be fit to a model that assumes only one sedimenting species. The simplified model will yield an average sedimentation coefficient and an overestimated diffusion coefficient that compensates for the spreading sedimenting boundary.

When s and D are well defined, the molecular mass and the shape of the sedimenting species can be determined by:

$$Mw = \frac{sRT}{D(1 - \bar{v}\rho)} \quad (2)$$

where R is the universal gas constant, $\bar{v}$ is the partial specific volume of the sedimenting species and ρ is the solvent density. With a distribution of sedimenting species, large uncertainties in the diffusion coefficient exist, and average sedimentation coefficients can be employed to estimate average molecular masses:

$$Mw \propto 6000s^{3/2} \quad (3)$$

Eq. 3 is an empirical relationship employed to estimate molecular masses of aqueous solutions of proteins (Chervenka, 1973).

Stafford (1992a,b) has developed another method for calculating the apparent sedimentation coefficient distribution, $g^*(s)_t$, for sedimenting species. This method does not retain any information regarding the diffusion coefficient of the sedimenting species. We employ the algorithm "dcdt" developed by Stafford to determine $g^*(s)_t$.

Dynamic light scattering

Dynamic light scattering (DLS) was performed on a Nicomp (Santa Barbara, CA) 370 instrument equipped with a Coherent (Santa Clara, CA) 304 argon ion laser. Samples were centrifuged to remove large material, and samples were analyzed for ~10 min. The results are presented as a mean Gaussian diameter (MGD). The cubic dependence of scattering on particle size (Andreu and Timasheff, 1986) causes the MGD to be biased toward larger-sized particles.

Kinetic measurements of aggregation

Aggregation kinetics were monitored after rapid manual dilution/mixing of the Aβ sample from a 30-mg/ml (6.5 mM) stock solution in DMSO or HFIP into the desired buffer. After dissolving the Aβ sample in DMSO, the solution was centrifuged at 10,000 × g for 5 min to remove undissolved material. Mixing was accomplished in the cuvette by rapidly drawing up and delivering the solution 10 to 15 times with a pipette equipped with a small-bore 200-μl disposable tip or by vortexing the sample immediately upon dilution. Final Aβ concentrations were kept in the range of 0.05–2.0 mg/ml (10–450 μM), with most measurements at 0.2 mg/ml (45 μM). Coaggregation and aggregation inhibition measurements were accomplished by premixing the stock DMSO solutions before dilution into the desired buffer. Seeding experiments were accomplished by mixing the seed Aβ sample into the desired buffer as described, allowing aggregation to occur, and then mixing in the secondary Aβ stock solution (dissolved in DMSO) as before.

Aggregation was monitored by following the change in turbidity with a Hewlett Packard (Palo Alto, CA) 8452 diode array spectrophotometer. Turbidity was monitored at 350 nm on unagitated samples in a cuvette with a 0.5–1.0-cm path length over the temperature range, 10–37°C. Unless otherwise noted, dilution of Aβ from its stock solution was accomplished immediately before the start of data collection (within 1 min). Turbidity measurements were compared with Rayleigh light-scattering measurements and similar behavior was observed.

Electron microscopy

Samples were collected from the aggregation kinetics experiments about one week after mixing. Samples (20 μl) were placed onto formvar carbon-coated specimen grids negatively stained with 2% phosphotungstic acid, and examined with a CM12 transmission electron microscope (TEM) operating at 80 kV accelerating voltage and 60,000× magnification.

RESULTS AND DISCUSSION

A paradigm for examining the aggregation of purified synthetic Aβ

The method we employ for monitoring Aβ aggregation behavior is to proceed from a clearly defined, monomeric starting state to a fibrillar final state. We start by characterizing the initial and final states and continue by monitoring the transition between these two states. In this approach the effects of added agents on the aggregation process are monitored during the transition.

RP-HPLC and ESI-MS were used as primary analytical methods to establish the purity of the peptide. Excellent synthetic results were obtained for the synthesis of Aβ40 with the desired product constituting at least 95% of the crude product. The purity level is equal to or better than the Aβ40 samples employed in various studies where analytical data for the peptides were given and comparisons could be made (Burdick et al., 1992). The synthesis of Aβ42 was more problematic, as unpurified peptide contained 80–85% of the desired material, with the remainder being truncated peptides. Routine purification of this peptide by HPLC to a single sequence was unreliable because of its extraordinarily poor

solubility and propensity to aggregate. These results are consistent with the results of others in which Aβ42 samples were produced by continuous solid-phase synthesis (Burdick et al., 1992). As a test of purity water-soluble and water-insoluble fractions of Aβ42 were compared by mass spectroscopy after centrifugation at 10,000 × *g*. No discernible differences between the samples were observed. These results indicate that our aggregation experiments are monitoring Aβ42 at the stated purity, not selectively monitoring more soluble impurities.

To assess the degree of aggregation of Aβ42 in potential purification solvents, we determined their MGD values by DLS (Table 1). The MGD provides a qualitative indication of aggregation but is strongly affected by presence of larger species, even at low concentrations. In DMSO the 10 mg/ml Aβ42 solution was >99% monomeric with an equivalent diameter of 2.4 nm. However, MGD values were skewed by a small population of large aggregates to yield mean values of 378 nm. Therefore the Aβ DMSO solutions were centrifuged for 10 min at 10,000 × *g* before use. When diluted into the other solvents, Aβ42 tended to aggregate with time. In either H_2O/TFA or ACN this trend of growing aggregate size was observed. Aggregation was particularly severe in solvent systems with trifluoroethanol exhibiting large size and rapid growth. The mixture, 50% ACN and 50% 2-propanol (2-Pr), yielded the smallest aggregate sizes and the most stable behavior. We are currently investigating ACN/2-Pr as a purification solvent for Aβ42.

One possible strategy considered for improving the purity of synthetic Aβ42 is a convergent fragment-coupling method rather than continuous solid-phase synthesis (Hendrix and Lansbury, 1992; Hendrix et al., 1992). The stated advantage of this approach is that the smaller component fragments can be highly purified before condensation, thereby limiting the number of peptides lacking one or two residues. In practice, however, fragment-coupling approaches suffer from both poor efficiency and yield. Finally, the potential for peptide racemization during consecutive condensations must also be addressed.

TABLE 1 Mean Gaussian diameter of 1 mg/ml Aβ42 in organic solvents at various ages

Solvent	Fresh (nm)	1.5 h (nm)	24 h (nm)
DMSO*			378‡
H_2O/0.1% TFA	36	96	263
ACN	27§	53	80
2-Pr	80§	96	187
TFE¶	134		180
50% ACN/50% 2-Pr	15		20
50% ACN/50% TFE	138		90
50% 2-Pr/50% TFE	47		87
10% TFE/0.1% TFA/H_2O	29§	108	1747
50% TFE/0.1% TFA/H_2O	1010§	406‖	410‖
70% TFE/0.1% TFA/H_2O	*	*	529

* In DMSO Aβ42 = 10 mg/ml. All other samples were prepared by diluting this starting solution tenfold with the indicated solvent. Therefore the Aβ42 = 1 mg/ml and there is 10% DMSO remaining.

‡ Analysis indicated that 99% of the sample had a diameter of 2.4 nm, which is probably monomer and the remainder distributed in the range 18–1000 nm.

§ Scattering intensity increased continuously, indicating rapid aggregation.

¶ trifluoroethanol

‖ It is likely that a large aggregate sedimented out of the cuvette and has been excluded from the measurement.

** Unstable scattering, probably due to severe aggregation during measurement.

Dissolution of the Aβ peptide and hydrodynamic characteristics of the initial and aggregated states

The aggregation states of Aβ stock solutions were characterized by analytical ultracentrifugation. Sedimentation equilibrium and velocity measurements for Aβ were compared in a series of stock solutions: DMSO, ACN/TFA, and H_2O (Figs. 1 and 2). Both Aβ40 and Aβ42 remained monomeric in DMSO over a wide concentration range (Fig. 1, *A* and *B*). After dispersion of solid peptide in ACN/TFA, a solvent composition commonly employed by researchers (Waite et al., 1992; Yankner et al., 1990), large aggregates were observed initially and increased in size over the course of several days (Fig. 1, *C* and *D*). Attempts to dissolve Aβ40 in distilled H_2O did not yield monomeric solutions; within 1–2 days molecular masses of ~8.5×10^5 Da developed with contributions from monomer representing less than 1% of the total content (Fig. 2 *A*). A sample that was aged for one month exhibited $s \sim 55$ S, which represents a molecular mass on the order of 2×10^6 Da (Fig. 2 *B*). The nonzero baseline in Fig. 2 *B* indicates that smaller species were also present, but they were not analyzed for size or contribution.

The aggregation states of Aβ40 and Aβ42 were further characterized in perdeuterated solvents, DMSO and ACN/DCl, by NMR (1 *D*). NMR spectra of Aβ40 in deuterated DMSO exhibited sharp lines that were concentration independent (in DMSO) over the range of 5–18 mg/ml (not shown). In comparison, in 30% deutrated ACN/0.1% DCl/D_2O, spectral lines were broad and concentration dependent across the same concentration range. These results are consistent with a monomeric form of Aβ in DMSO in comparison with an aggregated form in acidified ACN.

We also performed DLS measurements on solutions of Aβ40 and Aβ42 in HFIP (Pike et al., 1993), given that the solvent density of HFIP is too high ($\rho = 1.6$) to perform hydrodynamic measurements. At 30 mg/ml (6.5 mM), both Aβ40 and Aβ42 had diameters in the range 1.5–2 nm indicating that both Aβ40 and Aβ42 remained monomeric in HFIP. To date, HFIP and DMSO are the only solvents that we have observed to yield monomeric Aβ solutions reliably.

When an Aβ40 sample was aged in PBS at 450 μM (2 mg/ml), several ranges of species sizes were observed by hydrodynamic analysis (Fig. 3). At 3000 rpm (650 × *g*), large aggregates sedimented with $s \sim 50{,}000$ S (Fig. 3 *A*). These aggregates have molecular masses on the order of 10^{10} Da and are probably visible to the naked eye. Upon increase of the rotor velocity to 30,000 rpm (65,000 × *g*), a second species sedimented with $s \sim 30$ S (Fig. 3 *B*). This represents a smaller aggregate with a molecular mass of 10^6 Da, and therefore an aggregate of 1000 Aβ monomers. These latter aggregates are not removable from solution by a typical

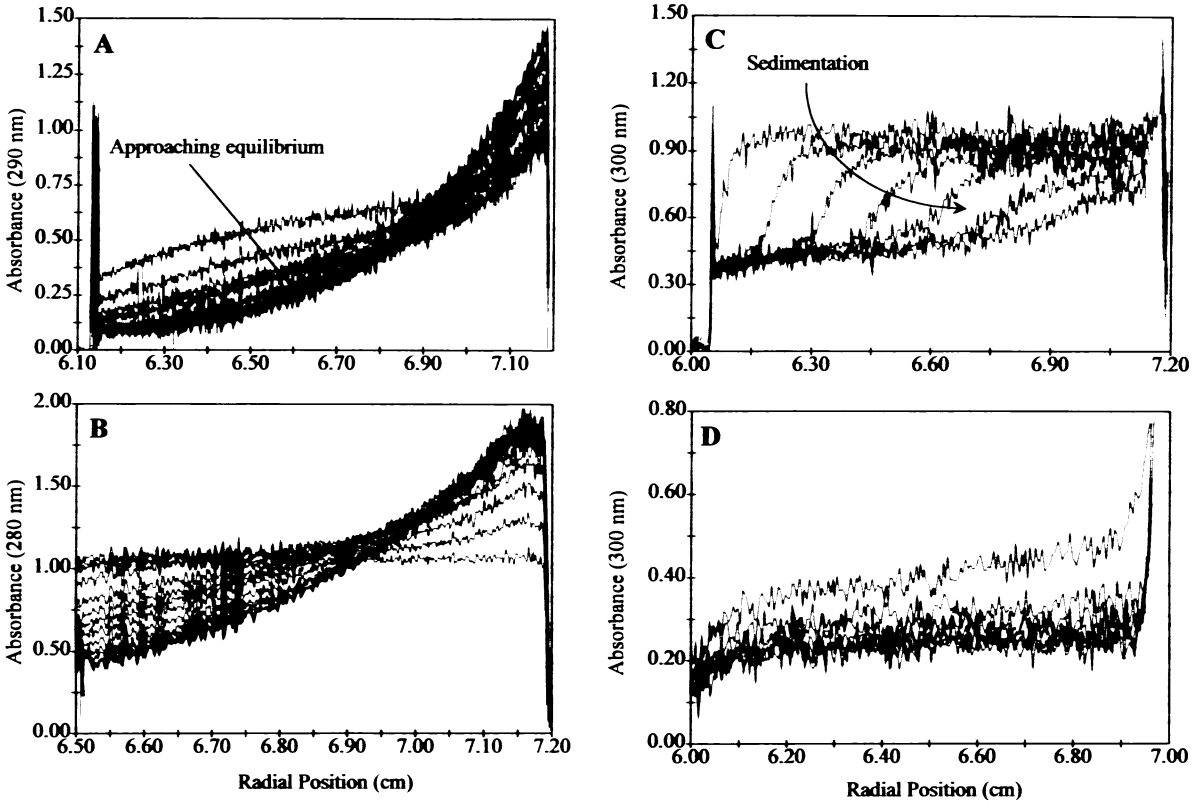

FIGURE 1 Sedimentation analyses of Aβ in different solvents. (*A*) Sedimentation equilibrium analysis of Aβ40 dissolved in DMSO at 3 mg/ml (690 μM), centrifuged at 60,000 rpm (250,000 × *g*) for 64 h (6-h intervals between scans) at 23°C. The spike at about 6.15 cm is the solution meniscus. To calculate the molecular weight for a sedimenting component, independent determination of the partial specific volume ($\bar{v}$) of the protein is required. A search of Chemical Abstracts (Chemical Abstract Services, American Chemical Society, Columbus, OH) did not reveal any earlier reports of determinations for proteins in DMSO. When we used the monomeric molecular weight observed by ESI-MS (4325 Da) for Aβ40 we calculated = 0.859 for monomer. To obtain dimer (8650 Da) required $\bar{v}$ = 0.884. (*B*) Sedimentation equilibrium analysis of Aβ42 dissolved in DMSO at 3 mg/ml (670 μM) under the same conditions as in (*A*) (at 4-h intervals). As with Aβ40 we used the molecular weight from ESI-MS (4511 Da) to estimate that $\bar{v}$ = 0.858 for Aβ42 in DMSO. Dimeric Aβ42 would require that $\bar{v}$ = 0.883. (*C*) Sedimentation velocity analysis of Aβ40 freshly dissolved in 30% ACN/0.1% TFA at 3 mg/ml centrifuged at 30,000 rpm (65,000 × *g*) for 1 h (at 12-min intervals) at 23°C. (*D*) Sedimentation velocity analysis of Aβ42 freshly dissolved in 30% ACN/0.1% TFA at 3 mg/ml centrifuged at 3000 rpm (650 × *g*) for 1 h (4-min intervals) at 23°C. The large amount of noise on the raw data could be attributed to oil deposits on the optical system of the XL-A ultracentrifuge. This noise limits our ability to estimate parameter uncertainties on the measurements, but does not perturb the trends in the results that we present.

microfuge centrifugation employed to remove insoluble material. We consider these species to be "soluble aggregates" that form an optically clear solution and can be easily mistaken for monomeric Aβ. Some material did not sediment at the higher rotor velocity; note that the baseline did not reach 0 at 30,000 rpm (Fig. 3 *B*). Analysis of the nonzero baseline indicated that the remaining material was monomeric.

As a comparison, Aβ40 was dissolved in DMSO and then diluted into PBS. After 3 days, the 230 μM Aβ solution exhibited an s ~30 S (data not shown), very similar to the soluble aggregates observed in the solution aged after direct dissolution in PBS. This size probably represents a size limit of "soluble aggregates" before larger structures were formed.

In a more detailed analysis (Fig. 4), the sedimentation velocity data at 30,000 rpm were fit to the model of Fujita (1962). The data could be fit better by a model that considered two sedimenting species rather than one (compare Fig. 4 *A* with 4 *B*). The two-component model yielded diffusion coefficients that correlated better with values expected from the aggregates sizes estimated from the sedimentation coefficients. Uncertainties in calculating the diffusion coefficient arise because the one component model must overestimate the diffusion coefficient to account for the boundary broadening that actually develops from the size distribution of aggregates (Holzman and Snyder, 1994). A comprehensive model of the aggregate sedimentation velocity behavior would likely encompass a Gaussian distribution of aggregate sizes based on polymer chain elongation (Demas and DeGraff, 1993). However, the signal-to-noise ratio for the Aβ sedimentation data was insufficient for such an approach, and it was not attempted.

The data were subjected to the analysis methods of Stafford (1992a,b) to calculate the apparent sedimentation coefficient distributions ($g^*(s)_t$; Fig. 5). The distribution exhibited a broad maximum in the region of s = 27 S with a full-width-half-maximum over the range, 17–42 S. Contributions decreased steadily with increasing s, and there was very little contribution from species with s <15 S. These

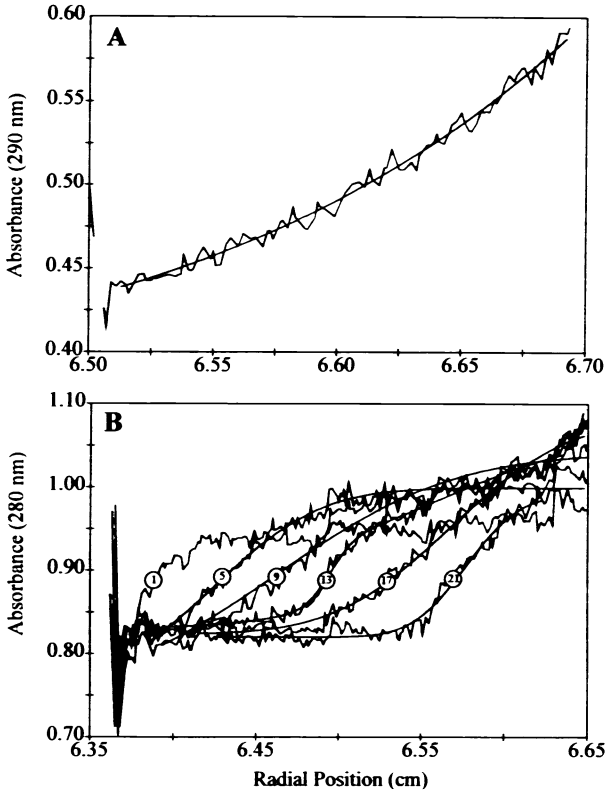

FIGURE 2 Sedimentation analyses of Aβ40 dissolved in distilled H_2O. (*A*) Sedimentation equilibrium analysis of 350 μM Aβ40 aged in H_2O for 1 day, centrifuged at 3000 rpm for 22 h at 23°C. Fitted curve through the data gave an Mw value of 8.5×10^5. (*B*) Sedimentation velocity analysis of 900 μM Aβ40 aged 1 month in H_2O analyzed at 3000 rpm, 23°C. Optical transients were collected at 4-h intervals at the indicated times. Solid thick lines through the data indicate the single-component fits to Eq. 1.

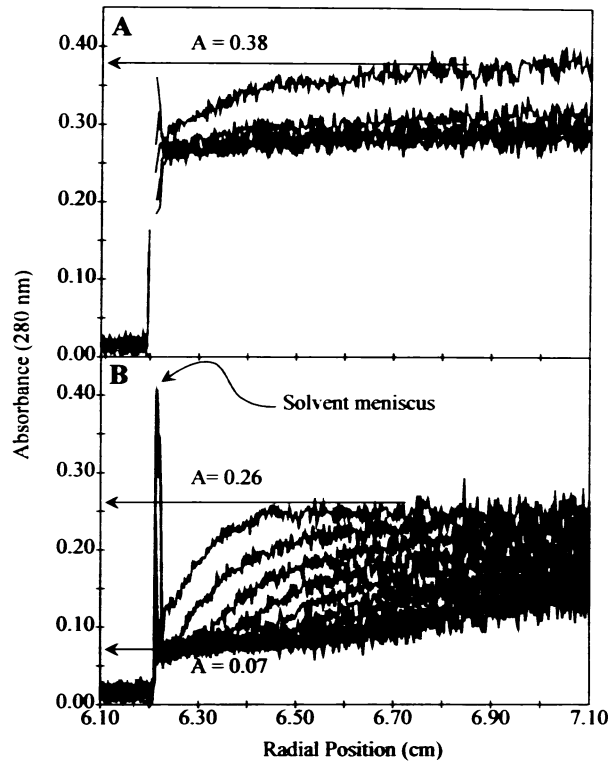

FIGURE 3 Aβ40 (2 mg/ml, 450 μM) dissolved and aged in PBS (50 mM phosphate, 150 mM NaCl, pH 7.40), 23°C. Optical transients collected at 280 nm. (*A*) Rotor velocity of 3000 rpm (650 × *g*) presented at 6-min intervals showing the sedimentation of large aggregates. Sedimentation analysis of these aggregates gave a sedimentation coefficient of 50,000 S. (*B*) Rotor velocity of 30,000 rpm (65,000 × *g*) presented at 4-min intervals showing the sedimentation of smaller, "soluble" aggregates. Analysis yielded *s* ~30 S. From the indicated absorbance the relative contributions of large aggregates, soluble aggregates, and small species can be estimated.

results suggest that the "soluble aggregate" forms a quasi-stable species with a finite distribution of aggregate sizes, and therefore that a distribution of aggregate sizes does not exist.

The form of the final aggregated state

Samples for transmission electron microscopy were taken directly from the samples prepared for analysis of aggregation kinetics. Densely packed fibrils were observed with Aβ40, Aβ40 M[O], and Aβ42. Fibrils had diameters of about 5 nm and lengths of about 100 nm (Fig. 6). In comparison, the reverse sequence 40–1 exhibited large amorphous globules when handled with identical procedures. The fibrillar structure for Aβ40 was similar at pH 4.1 and pH 7.4 (not shown).

Kinetics of amyloid aggregation.

Monitoring Aβ aggregation by turbidity measurements provides a picture of the overall concentration of aggregated peptide. Choice of wavelength affects the subset of sizes that are monitored (Doty and Steiner, 1950), but little information regarding the number, size, or shape of the aggregates can be discerned from single-wavelength, single-angle presentation. However, from the time-dependent change in the signal, the rate that small Aβ species enter the aggregated state can be followed. We present these results without modeling the kinetics as a guide to monitoring Aβ aggregation behavior.

In Fig. 7, we present a comparative pH study of the aggregation kinetics of the Aβ40, Aβ40 M[O], and Aβ42. For Aβ40, aggregation was rapid (seconds) at pH 5 and 6, whereas at pH 4 it was slow (hours). At pH 7.0 and 7.40, aggregation was extremely slow (days). Aβ40 M[O] exhibited similar behavior as its unmodified analog, but kinetics were faster in all cases. Aβ42 aggregated more rapidly than Aβ40 over the entire pH range investigated; complete aggregation was observed within 1 min at all pH values studied. The aggregation kinetics of Aβ 1–43 were very similar to Aβ42 (data not shown).

The dramatic enhancement of aggregation rate observed with Aβ42, in comparison with Aβ40, suggests that the hydrophobic carboxy terminus of Aβ plays a critical role in aggregation. Lansbury and co-workers (Spencer et al., 1991; Jarrett and Lansbury, 1993; Jarrett et al., 1993) have suggested that structural ordering of the carboxy terminus is the rate-determining step for Aβ aggregation. The pH dependence of the kinetics reveals that the charged amino terminus and central region of the peptide must also be involved in

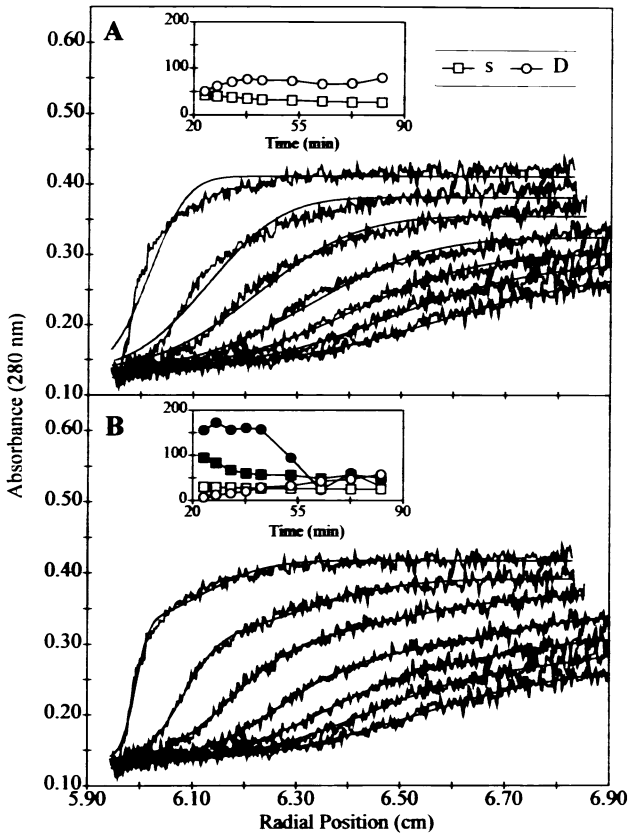

FIGURE 4 Analysis of sedimentation velocity data for 2 mg/ml (450 μM) Aβ40 dissolved and aged in PBS (50 mM phosphate, 150 mM NaCl, pH 7.40), 30,000 rpm (65,000 × *g*), 23°C (5-min intervals). (*A*) Solid thick lines through the data indicate the single component fits. (*Inset*) Analysis of data of (poor) single-component fits for sedimentation and diffusion coefficients according to Eq. 1. Sedimentation coefficient, in Svedbergs (□) and diffusion coefficient (○) in Ficks. The analysis yielded an average s = 32 S and an average d = 72 F. The magnitude of the diffusion coefficient does not correlate well with the sedimentation coefficient. (*B*) Reanalysis (solid thick lines) of the identical data with a two-component fit for sedimentation and diffusion coefficients according to Eq. 1. (*Inset*) Analysis of data from two-component fits of sedimentation and diffusion coefficients according to Eq.1. Solid thick lines through the data indicate the (good) two-component fits. The analysis yielded two components with a 2:1 contribution with s = 28 and 64 S, respectively. The diffusion coefficients were still overestimated (35 and 110 F), indicating that although the fit quality seemed satisfactory, there was a failure to fit a model with discrete components.

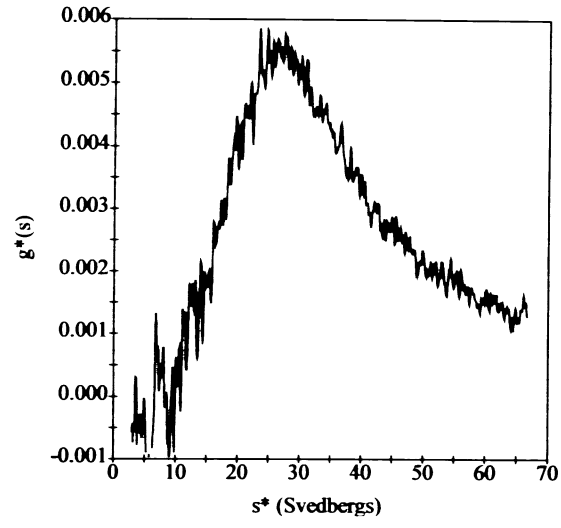

FIGURE 5 Apparent sedimentation coefficient distribution ($g^*(s)_r$) as a function of sedimentation coefficient. The data from Fig. 4 were fit using "dcdt" from Stafford (1992a,b) over the time range 38–63 min with Δt = 15 min. $g^*(s)_r$ exhibited a broad maximum near s = 27 S and a full-width-half-maximum over the range 17–42 S. The analysis is uncorrected for diffusion.

aggregation. Given our findings that Aβ40 M[O], which contains a more polar group in the middle of the hydrophobic region, aggregates faster than the normal peptide, it may be premature to focus solely on the conformation of the carboxy terminal residues as controlling the rate of aggregation. Aggregation likely requires interactions along much of the Aβ chain. An antiparallel β-sheet requires head-to-tail orientation so the carboxy terminus cannot exclusively control aggregation.

We have other corroborating evidence indicating that aggregation is dependent upon much of the Aβ sequence. Chemical modification of Aβ40 inhibited aggregation under conditions where unmodified Aβ40 readily aggregated. Both conjugation of fluorescein to the amino terminal Asp-1 and iodination of Tyr-10 inhibited aggregation (data not shown). These modifications are remote from the carboxyl terminus of Aβ and further point to the involvement of the entire molecule in controlling aggregation.

To understand further the factors that control Aβ aggregation, we studied the starting solvent, concentration, temperature, and ionic strength effects on aggregation kinetics. In Fig. 8, we show that Aβ40 aggregation kinetics exhibit a strong nonlinear dependence on peptide concentration. Aggregation exhibits threshold-type behavior, where rates are dramatically enhanced once a given sample concentration is reached. This behavior indicates that the rate-determining step is the formation of a multimeric seed or initiator (Hofrichter et al., 1974; Jarrett and Lansbury, 1992, 1993).

When starting from HFIP, a solvent in which Aβ40 remains monomeric, aggregation kinetics increased by a factor of ~10 in comparison with DMSO (Fig. 8 *B*). In HFIP, Aβ is reported to be a mixture of random coil and α-helix with little-to-no β-sheet character (Hilbich et al., 1991; Barrow et al., 1992). Increased aggregation probably arises from the decreased hydrogen bonding, and therefore, decreased solvation by HFIP. This variation in aggregation behavior portends the difficulties in correlating Aβ aggregation and structure to toxicity.

The dependence of Aβ40 aggregation on solution ionic strength is presented in Fig. 9 for a series of NaCl concentrations (0–500 mM). Aggregation is strongly accelerated by increasing salt concentration, again revealing the dependence of aggregation properties on handling conditions. In addition, aggregation is weakly dependent upon temperature, increasing as the temperature is raised from 10 to 37°C (data

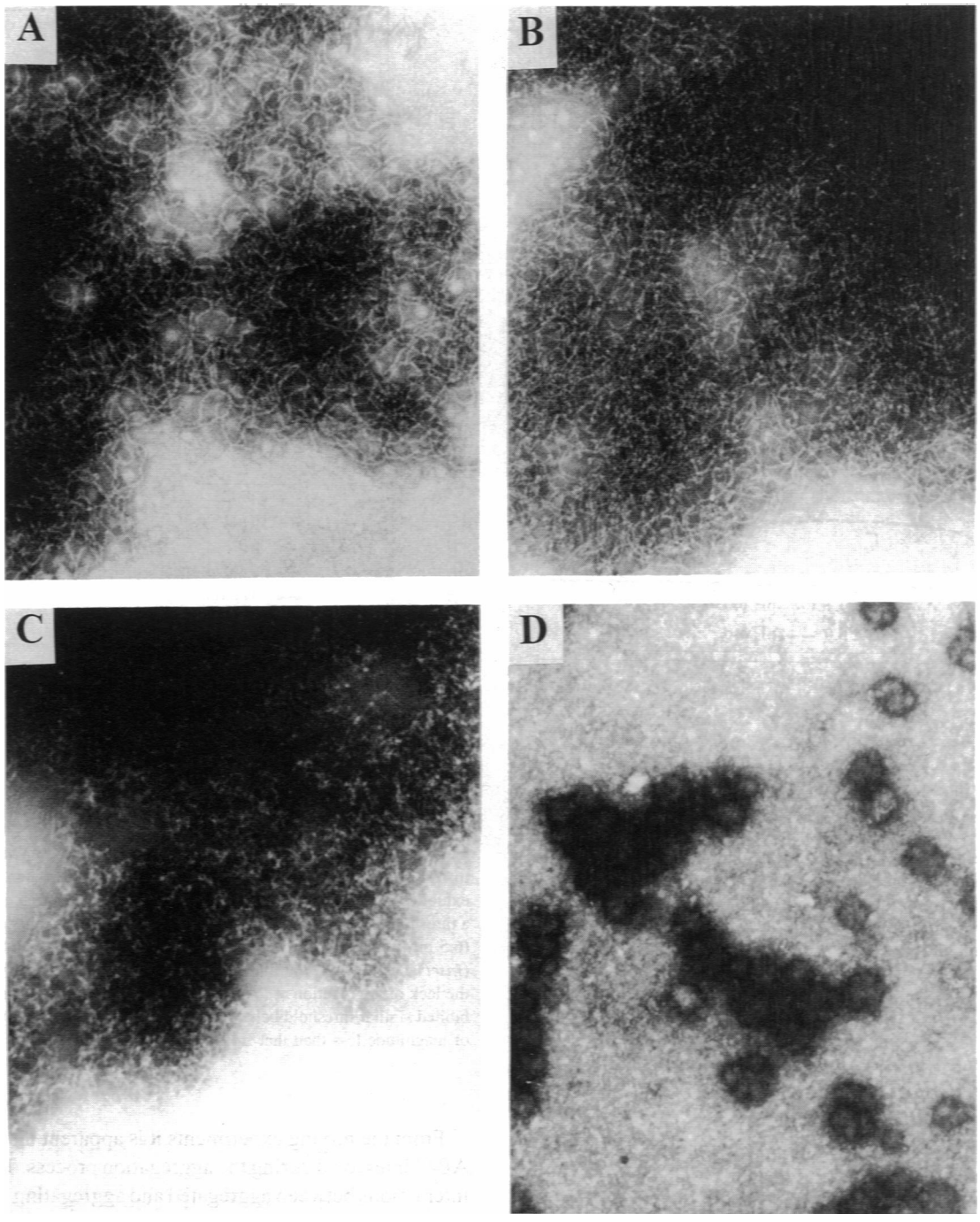

FIGURE 6 Transmission electron micrographs of (*A*) Aβ40, (*B*) Aβ40 M[O], (*C*) Aβ42, and (*D*) 40–1 peptide. Samples were diluted out of DMSO into the wide-range pH buffer at pH 4.1 and aged for 1 week at 45 μM. Individual samples were placed on formvar carbon specimen grids and negatively stained with 2% phosphotungstic acid for 1 min. All grids were examined with a CM12 TEM operating at 80 kV and 60,000× magnification. Intertwined fibrils of about 5 nm diameter and variable lengths (~100 nm) were observed in all three Aβ samples. With the reverse sequence 40–1, only amorphous globs were observed.

not shown). Taken together, the ionic strength and temperature dependence indicate that aggregation is driven by a hydrophobic effect (Hilbich et al., 1991).

Inhibition of Aβ42 aggregation and seeding of Aβ40 aggregation. Given the large differences in aggregation rates for Aβ40 and Aβ42 under identical conditions, we investigated the aggregation rates when Aβ40 and Aβ42 were mixed at several pH values (Fig. 10 *A*) and peptide concentrations (Fig. 10 *B*). A significant concentration-dependent decrease in rate was observed for Aβ42 aggregation when the two were mixed. With the mixture, the turbidity signal increased from an early time level near baseline without the rapid rise observed for Aβ42 by itself. These results cannot be attributed to rapid aggregation of Aβ42 followed by a

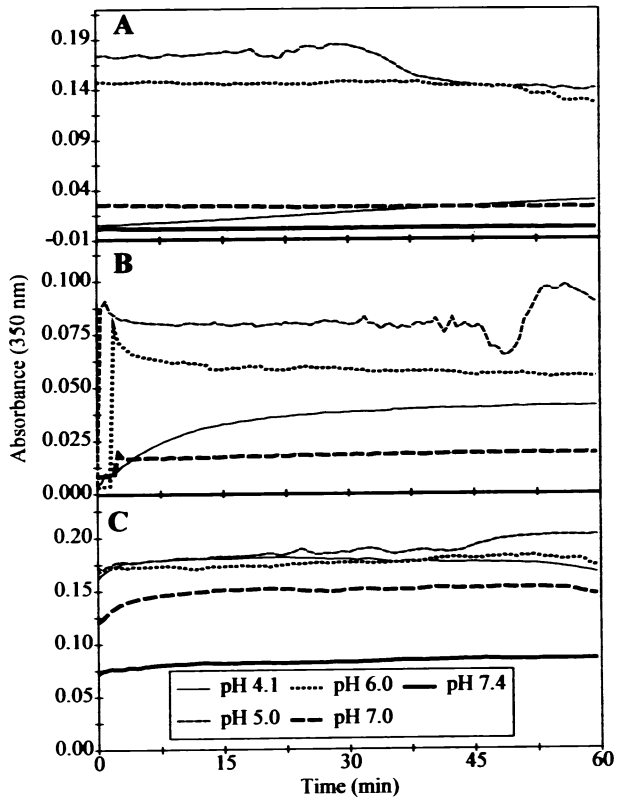

FIGURE 7 Aggregation kinetics of (*A*) Aβ40, (*B*) Aβ40 M[O], (*C*) Aβ42 at several pH values. Samples were diluted out of DMSO at 30 mg/ml (6.5 mM) to a final concentration of 0.2 mg/ml (45 μM) in either the wide-range pH buffer (pH 4.1, 5.0, 6.0, and 7.0) or PBS (10 mM phosphate, 150 mM NaCl, pH 7.40) and rapidly mixed. Turbidity was monitored in 0.5-cm path length cells at 37°C with an HP8452 diode array spectrophotometer. Dilution from DMSO into buffer was performed about 30 s before the start of data collection. In cases where aggregation was rapid (seconds), shifts in turbidity were frequently observed (e.g., Aβ40 M[O] at pH 5.0), which can probably be attributed to settling of large aggregates.

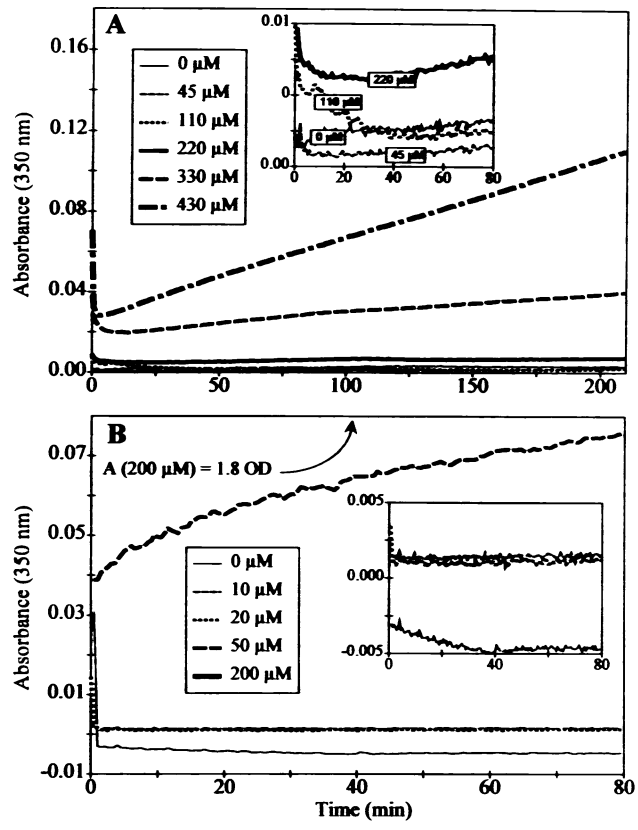

FIGURE 8 Concentration dependence of aggregation kinetics of Aβ40 in PBS (10 mM phosphate, 150 mM NaCl, pH 7.40). Turbidity was monitored in 1.0-cm path length cells at 350 nm at 20°C. (*A*) Aβ40 was diluted out of DMSO at 30 mg/ml to the indicated concentrations, 45–430 μM (0.2–>2 mg/ml). (*Inset*) The low concentration regime (≤ 220 μM) is expanded to reveal the lack of aggregation at the low concentrations. Aggregation exhibited a strong nonlinear dependence upon concentration, indicating that a threshold exists for rapid aggregation. (*B*) Aβ40 was diluted out of HFIP (6.5 mM) to the indicated concentrations, 10–200 μM (0.04–0.8 mg/ml). (*Inset*) The low concentration regime (≤ 20 μM) was expanded to reveal the lack of aggregation at low concentrations. Aggregation from HFIP exhibited similar threshold behavior, but at concentrations that were an order of magnitude less than that from DMSO.

seeding of Aβ40 aggregation by aggregated Aβ42. Instead, the rate retardation observed with a mixture of Aβ42 and Aβ40 must be attributed to inhibition of Aβ42 aggregation when the two are mixed together.

We continued these mixing experiments by investigating the effect of several Aβ fragments (1–28, 25–35, 30–40, and 30–42) or the reverse sequence peptide (40–1) on aggregation kinetics of Aβ42 (Fig. 11). Only a slight inhibition of aggregation was observed in most cases. This is probably due to nonspecific interactions between intact Aβ42 and the fragments (or 40–1). There was also only a slight inhibition of aggregation in the presence of 20% bovine serum albumin (data not shown). Aβ 1–28 was intermediate in its effectiveness at inhibiting Aβ42 aggregation (Fig. 11). A combination of Aβ fragments, 1–28 and 30–40, (also 30–42), did not retard Aβ42 aggregation to any greater extent than the separate fragments; in fact, inhibition was less than that observed for intact Aβ40. Taken together these data suggest that both specific inhibition of aggregation, and aggregation itself, required interactions along the whole peptide sequence.

From the mixing experiments it is apparent that Aβ40 and Aβ42 interacted during the aggregation process. To study the interactions between aggregated and aggregating peptide, we studied the ability of preformed aggregates of Aβ42 to seed the aggregation of 45 μM Aβ40 (Fig. 12). By itself Aβ40 aggregates very slowly (Fig. 12 *A*). In the presence of 11 μM aggregated Aβ42, the rate of Aβ40 aggregation increased dramatically (minutes, Fig. 12 *B*), and in the presence of 45 μM Aβ42, Aβ40 aggregated in seconds (Fig. 12 *C*). In Fig. 12 *D* we show that the increase in turbidity observed in Fig. 12 *C* cannot be attributed to agitation of aggregated Aβ42 that has deposited in the cuvette. Therefore, aggregation of Aβ40 is enhanced by several orders of magnitude in a dose-dependent fashion when seeded with aggregated Aβ42. As we first noted (Snyder et al. 1993a) and as confirmed by Jarrett et al. (1993), aggregated Aβ42 is capable of initiating the polymerization of Aβ40.

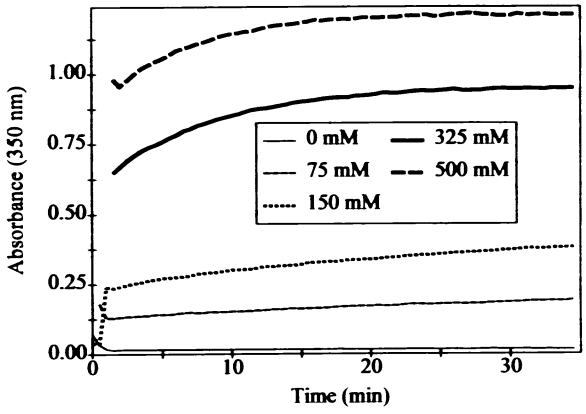

FIGURE 9 Ionic strength dependence of the aggregation kinetics of Aβ40 diluted from HFIP into PBS (10 mM phosphate, pH 7.40) and varying concentrations of NaCl (0–500 mM). Turbidity was monitored in 1-cm path length cells at 350 nm at 20°C at 68 μM Aβ40. Aggregation was strongly dependent upon salt concentration, again exhibiting threshold behavior. The salt concentration required for rapid aggregation was much smaller at higher Aβ40 concentrations (data not shown).

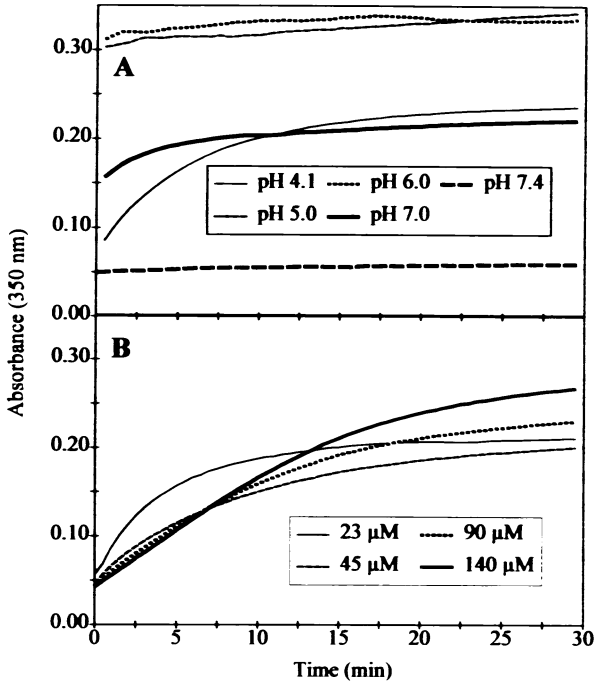

FIGURE 10 Aggregation kinetics of Aβ42 mixed with Aβ40. The two Aβ samples were mixed in DMSO (each at 15 mg/ml) and diluted into either the wide-range buffer or PBS (10 mM phosphate, 150 mM NaCl, pH 7.40). Turbidity was monitored in 0.5-cm path length cells at 37°C. (*A*) Dependence of inhibition of aggregation on pH at 4.1, 5.0, 6.0, 7.0, and 7.4) on samples with 0.2 mg/ml (45 μM) of both Aβ40 and Aβ42. (*B*) Concentration dependence of the inhibition of aggregation at pH 7.0. Aβ42 concentrations were held at 0.2 mg/ml, whereas Aβ40 concentrations were varied between 0.1–0.6 mg/ml (23–140 μM).

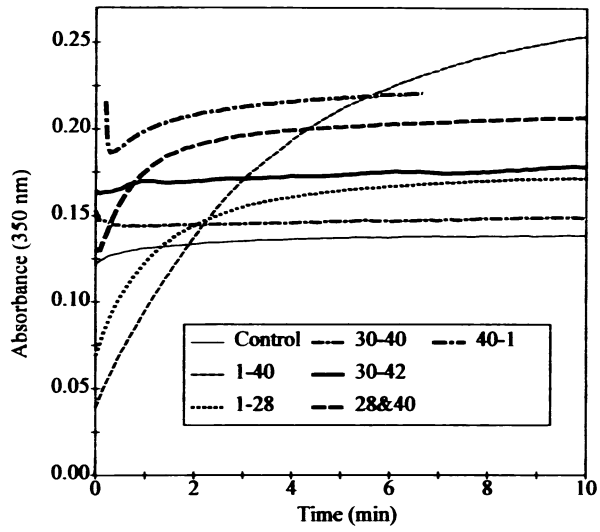

FIGURE 11 Inhibition of Aβ42 aggregation by the indicated Aβ fragments (or the 40–1 peptide) mixed in DMSO and diluted into pH 7.0 wide-range buffer. Turbidity was monitored in 0.5-cm path length cells at 37°C. All peptide concentrations were held at 50 μM. The control had Aβ42 without any added fragments. Aβ40 had the most dramatic effect on Aβ42 aggregation. Aβ 1–28 had an intermediate effect, and the smaller Aβ fragments and 40–1 had only small effects. The combination of Aβ 1–28 and 30–40 inhibited Aβ42 aggregation to the same degree as Aβ 1–28 by itself.

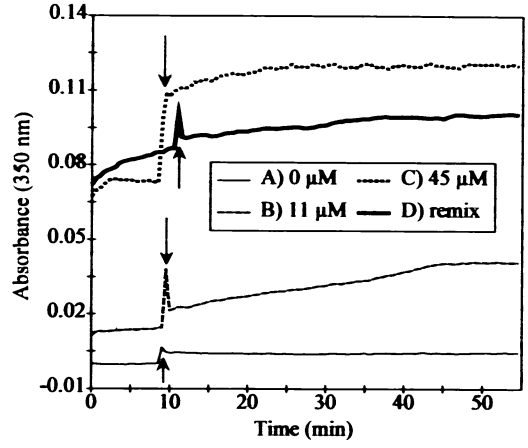

FIGURE 12 Seeding of 0.2 mg/ml (45 μM) Aβ40 aggregation by Aβ42 in PBS (10 mM phosphate, 150 mM NaCl, pH 7.40). Aβ42 was diluted from DMSO (30 mg/ml) and allowed to aggregate for 1 h at 0.2 mg/ml (45 μM) in PBS at 37°C. Aβ40 was diluted from DMSO (30 mg/ml) into the indicated solutions. Turbidity was monitored on 1.0-cm path length cells at 23°C. *A*) Aβ40 diluted into PBS without Aβ42. *B*) Aβ40 diluted into 0.05 mg/ml (11 μM) Aβ42 (aggregated at 0.2 mg/ml). (*C*) Aβ40 diluted into 0.2 mg/ml (45 μM) Aβ42. Aggregation kinetics of Aβ40 are enhanced by the presence of aggregated Aβ42 in a dose-dependent manner. (*D*) The aggregated 0.2 mg/ml (45 μM) Aβ42 solution was remixed in the same fashion as Aβ40 was added, but no addition of concentrated Aβ40 was performed. This remixing of aggregated Aβ42 did not increase the signal as observed with addition of nonaggregated Aβ40.

Factors controlling the aggregation/polymerization process

The rate of Aβ aggregation is controlled by two distinct factors. First, solution conditions that decrease solubility and/or increase β-sheet character accelerate aggregation kinetics; aggregation is controlled by the ability of the appending monomer to acquire the required structure for polymerization. Lansbury (1992) has suggested that the two additional

residues on Aβ42, Ile-Ala, drive the carboxy terminus toward an extended β-sheet structure that is limited by a *cis*-amide isoform at Gly37-Gly38 (Spencer et al., 1991). This can be seen in the accentuated aggregation rates of Aβ42 in comparison with Aβ40.

Second, aggregation rates are controlled by the number of sites available for elongation. Aβ aggregation/polymerization exhibits lag time and threshold behavior observed with polymerization processes (Hofrichter et al., 1974; Jarrett and Lansbury, 1992, 1993). Once nucleating sites are available, Aβ aggregates rapidly. In the experiments with mixed Aβ40 and Aβ42, aggregation kinetics were inhibited because Aβ40 prevented nuclei of Aβ42 multimers from forming, by a competitive binding mechanism. This effect is transient in nature because, once the nucleating species are formed, both Aβ42 and Aβ40 aggregate. In fact, when more Aβ40 is present, kinetics are retarded, but the overall turbidity signal rises well above samples without Aβ40.

From the dependence of Aβ aggregation kinetics on the ratio of Aβ40 and Aβ42, we speculate that the amount of accumulated peptide might correlate more closely with either the relative ratio of the longer to shorter forms of Aβ than to overall Aβ concentration. Cerebrospinal fluid concentrations of Aβ40 are in the range from high picomolar to low nanomolar (Seubert et al., 1992; Shoji et al., 1992), significantly below threshold concentrations required for rapid aggregation (~350 μM). Considering its sluggish aggregation rates, unless high concentrations of Aβ40 develop in localized regions, it is unlikely that a significant amount of Aβ40 would aggregate by itself. On the other hand, aggregates of Aβ42 or mixtures of Aβ42 and Aβ40 that aggregate in the seconds-to-minutes time regime would more readily develop in vivo. This leads to questions regarding cleavage specificity of the carboxy terminus of βPP. Slight changes in differential processing of the carboxy terminus could have dramatic effects on the amount of Aβ aggregation and accumulation.

Another factor that can affect aggregation rates is the degree of Met-35 oxidation in Aβ40 (or possibly Aβ42). In a comparison of aggregation rates for Aβ40 versus Aβ40 M[O] (Fig. 7), Met oxidization enhanced aggregation rates. Oxidation of Aβ by radical damage has been suggested as a causative agent to Aβ toxicity (Behl et al., 1992; Dyrks et al., 1992; Hensley et al., 1994); increased aggregation rates could contribute to increased toxicity.

Much of the variance observed in Aβ toxicity could be due to the extreme sensitivity of the aggregation process to handling conditions. We have shown that several factors (i.e. Aβ concentration, pH, and ionic strength) require only slight modification to change aggregation rates dramatically. The trends in aggregation behavior that we have presented are a paradigm, but ultimately Aβ toxicity should be correlated with the aggregation state of the specific samples investigated. Consideration of the aggregation process during experimental design will avail the investigator increased reproducibility in toxicity assays.

CONCLUSIONS

We have developed a paradigm for studying the aggregation behavior of Aβ as it proceeds from a monomeric starting state to a fibrillar final state. Aβ40 and Aβ42 remain monomeric in DMSO or HFIP up to millimolar concentrations but aggregate heavily in water, PBS, or ACN/TFA, at submillimolar concentrations. In PBS, aggregated Aβ40 forms several types of species, including large, probably visible, aggregates with a sedimentation coefficient of ~50,000 S, small, soluble aggregates with s ~30 S, and monomer. Aggregation kinetics are strongly dependent upon sample and environmental conditions. Aggregation is very rapid (seconds) near the pI of the peptide (pH 5–6). Outside of this range, aggregation of Aβ42 remains rapid (minutes), whereas Aβ40 aggregation slows (hours to days). Aβ aggregation exhibits ionic strength and temperature dependence indicative of an aggregation being driven by a hydrophobic effect. In addition, aggregation of Aβ40 displays threshold-type behavior, which indicates that the rate-determining step is the formation of a multimeric seed. When mixed together as monomers, Aβ40 (or other Aβ fragments) and Aβ42 aggregate at a rate much slower than Aβ42 by itself. This retardation of aggregation rate is dose dependent and is observed most specifically for Aβ40. As less of the intact Aβ structure is retained, peptides are less competent to inhibit Aβ42 aggregation. In addition, preformed aggregates of Aβ42 are capable of seeding Aβ40 aggregation in a dose-dependent fashion. The interplay in the aggregation kinetics of Aβ40 and Aβ42 suggests that relative concentrations of Aβ42 could be a factor in Aβ deposition.

The authors thank Dr. Thomas Perun for his support and encouragement in Pharmaceutical Discovery Research at Abbott Laboratories. Electron microscopy was performed by the Cellular and Microscopic Research group at Abbott Laboratories under the direction of Dr. M. Miller. NMR was performed by Dr. Y. Theriault and Dr. S. Fesik, and mass spectroscopy was performed by Dr. A. Buko, all of Abbott Laboratories. We thank all for their assistance. We thank Dr. W Stafford (Boston Biomedical Research Institute) for use of "dcdt" software.

This work was supported in part by National Institutes of Health NIA grant AG10481.

REFERENCES

Andreu, J. M., and S. N. Timasheff. 1986. The measurement of cooperative protein self-assembly by turbidity and other techniques. *Methods Enzymol.* 130:47–59.

Barrow, C. J., A. Yasuda, P. T. M. Kenny, and M. G. Zagorski. 1992. Solution conformations and aggregational properties of synthetic amyloid beta-peptides of Alzheimer's disease. Analysis of circular dichroism spectra. *J. Mol. Biol.* 225:1075–1093.

Behl, C., J. Davis, G. M. Cole, and D. Schubert. 1992. Vitamin E protects nerve cells from amyloid β-protein toxicity. *Biochem. Biophys. Res. Commun.* 186:944–950.

Burdick, D., B. Soreghan, M. Kwon, J. Kosmoski, M. F. Knauer, A. Henschen, J. Yates, C. Cotman, and C. G. Glabe. 1992. Assembly and aggregation properties of synthetic Alzheimer's A4/beta amyloid peptide analogs. *J. Biol. Chem.* 267:546–554.

Caputo, C. B., P. E. Fraser, I. E. Sobel, and D. A. Kirschner. 1992. Amyloid-like properties of a synthetic peptide corresponding to the carboxy terminus of β-amyloid protein precursor. *Arch. Biochem. Biophys.* 292: 199–205.

Caputo, C. B., I. R. E. Sobel, L. A. Sygowski, R. A. Lampe, and R. C. Spreen. 1993. The influence of amino-acid-sequence on the fibrillogenicity and amyloidogenicity of the carboxy-terminus of β-amyloid precursor protein. *Arch. Biochem. Biophys.* 306:321–330.

Chervenka, C. H. 1973. A Manual of Methods for the Analytical Ultracentrifuge. Palo Alto, Spinco Divsion, Beckman Instruments.

Demas, J. N., and B. A. DeGraff. 1993. Luminescence-based sensors: microheterogeneous and temperature effects. *Sensors and Actuators B* 11: 35–41.

Doty, P., and R. F. Steiner. 1950. Light scattering and spectrophotometry of colloidal solutions. *J. Chem. Phys.* 18:1211–1220.

Fraser, P. E., J. T. Nguyen, W. K. Surewicz, and D. A. Kirschner. 1991. pH-dependent structural transitions of Alzheimer amyloid peptides. *Biophys. J.* 60:1190–1201.

Fraser, P. E., J. T. Nguyen, H. Inouye, W. K. Surewicz, D. J. Selkoe, M. B. Podlisny, and D. A. Kirschner. 1992. Fibril formation by primate, rodent, and Dutch-hemorrhagic analogues of Alzheimer amyloid beta-protein. *Biochemistry.* 31:10716–10723.

Fujita, H. 1962. Mathematical Theory of Sedimentation Analysis. New York, Academic Press.

Giordano, T., J. B. Pan, L. M. Monteggia, T. F. Holzman, S. W. Snyder, G. A. Krafft, H. Ghanbari, and N. W. Kowall. 1994. Similarities between beta amyloid peptides 1–40 and 40–1: effects on aggregation, toxicity, in vitro, and injection in young and aged rats. *Exp. Neurol.* 125:175–182.

Glenner, G. G. 1980. Amyloid deposits and amyloidosis: the beta fibrilloses 1. *N. Engl. J. Med.* 302:1283–1292.

Glenner, G. G., and C. W. Wong. 1984. Alzheimer's disease and Down's syndrome: sharing of a unique cerebrovascular amyloid fibril protein. *Biochem. Biophys. Res. Commun.* 122:1131–1135.

Gorevic, P. D., P. C. Munoz, T. T. Casey, C. R. Diraimondo, W. J. Stone, F. C. Prelli, M. M. Rodrigues, M. D. Poulik, and B. Frangione. 1986. Ten to fourteen residue peptides of Alzheimer's disease protein are sufficient for amyloid fibril formation and its characteristic x-ray diffraction pattern. *Proc. Natl. Acad. Sci. USA.* 83:7908–7912.

Goldgaber, D., M. I. Lerman, W. O. McBride, U. Saffiotti, and C. D. Gajdusek. 1987. Characterization and chromosomal localization of a cDNA encoding brain amyloid of Alzheimer's disease. *Science.* 235:877–880.

Haass, C., M. G. Schlossmacher, A. Y. Hung, C. Vigo-Pelfrey, A. Mellon, B. L. Ostaszewski, I. Lieberburg, E. H. Koo, D. Schenk, D. B. Teplow, and D. J. Selkoe. 1992. Amyloid β-peptide is produced by cultured cells during normal metabolism. *Nature.* 359:322–325.

Halvserson, K. J., P. E. Fraser, D. A. Kirschner, and P. T. Lansbury Jr. 1990. Molecular determinants of amyloid deposition in Alzheimer's disease: conformation studies of synthetic beta-protein fragments. *Biochemistry.* 29:2639–2644.

Hendrix, J. C., K. J. Halvserson, and P. T. Lansbury Jr. 1992. A convergent synthesis of the amyloid protein of Alzheimer's disease. *J. Am. Chem. Soc.* 114:7930–7931.

Hendrix, J. C., and P. T. Lansbury Jr. 1992. Synthesis of a protected peptide corresponding to residues 1–25 of the beta-amyloid protein of Alzheimer's-disease. *J. Org. Chem.* 57:3421–3426.

Hensley, K., J. M. Carney, M. P. Mattson, M. Aksenova, M. Harris, J. F. Wu, R. A. Floyd. 1994. A model for β-amyloid aggregation and neurotoxicity based on free radical generation by the peptide: relevance to Alzheimer disease. *Proc. Natl. Acad. Sci. USA.* 91:3270–3274.

Hilbich, C., B. Kisters-Woike, J. Reed, C. L. Masters, and K. Beyreuther. 1991. Aggregation and secondary structure of synthetic amyloid beta A4 peptides of Alzheimer's disease. *J. Mol. Biol.* 218:149–163.

Hofrichter, J., P. D. Ross, and W. A. Eaton. 1974. Kinetics and mechanism of deoxyhemoglobin S gelation: a new approach to understanding sickle cell disease. *Proc. Natl. Acad. Sci. USA.* 71:4864–4868.

Holzman, T. F., and S. W. Snyder. 1994. Applications of analytical ultracentrifugation in structure-based drug design. *In* Modern Analytical Ultracentrifugation: Acquisition and Interpretation of Data for Biological and Synthetic Polymer Systems. T. M. Schuster, T. M. Laue, editors. Boston, Birkhauser Division, Springer-Verlag.

Hyman, B. T., K. Marzloff, and P. V. Arriagada. 1993. The lack of accumulation of senile plaques or amyloid burden in Alzheimers-disease suggests a dynamic balance between amyloid deposition and resolution. *J. Neuropathol. Exp. Neurol.* 52:594–600.

Inouye, H., P. E. Fraser, and D. A. Kirschner. 1993. Structure of beta-crystalline assemblies formed by Alzheimer beta-amyloid protein analogues: analysis by x-ray diffraction. *Biophys. J.* 64:502–519.

Jarrett, J. T., E. P. Berger, and P. T. Lansbury Jr. 1993. The carboxy terminus of the beta-amyloid protein is critical for the seeding of amyloid formation: implications for the pathogenesis of Alzheimers-disease. *Biochemistry.* 32:4693–4697.

Jarrett, J. T., and P. T. Lansbury Jr. 1992. Amyloid fibril formation requires a chemically discriminating nucleation event: studies of an amyloidogenic sequence from the bacterial protein OsmB. *Biochemistry.* 31:12345–12352.

Jarrett, J. T., and P. T. Lansbury Jr. 1993. Seeding one-dimensional crystallization of amyloid: a pathogenic mechanism in Alzheimers-disease and scrapie. *Cell.* 73:1055–1058.

Kang, J., H. Lemaire, A. Unterbeck, J. M. Salbaum, C. L. Masters, K. H. Grzeschik, G. Multhaup, K. Beyreuther, and B. Muller-Hill. 1987. The precursor of Alzheimer's disease amyloid A4 protein resembles a cell-surface receptor. *Nature.* 325:733–736.

Kirschner, D. A., C. R. Abraham, and D. J. Selkoe. 1986. X-ray diffraction from intraneuronal paired helical filaments and extraneuronal amyloid fibers in Alzheimer disease indicates cross-beta conformation. *Proc. Natl. Acad. Sci. U.S.A.* 86:503–507.

Kirschner, D. A., H. Inouye, L. K. Duffy, A. Sinclair, M. Lind, and D. J. Selkoe. 1987. Synthetic peptide homologous to beta protein from Alzheimer disease forms amyloid-like fibrils in vitro. *Proc. Natl. Acad. Sci. USA.* 84:6953–6957.

Kitaguchi, N., Y. Takahashi, Y. Tokushima, S. Shiojiri, and H. Ito. 1988. Novel precursor of Alzheimer's disease amyloid protein shows protease inhibitory activity. *Nature.* 331:530–532.

Knauer, M. F., B. Soreghan, D. Burdick, J. Kosmoski, and C. G. Glabe. 1992. Intracellular accumulation and resistance to degradation of the Alzheimer amyloid A4/beta protein. *Proc. Natl. Acad. Sci. USA.* 89:7437–7441.

Kowall, N. W., F. M. Beal, J. Busciglio, L. K. Duffy, and B. A. Yankner. 1991. An in vitro model for the neurodegenerative effects of β amyloid and protection by substance P. *Proc. Natl. Acad. Sci. USA.* 88: 7247–7251.

Krafft, G. A. 1993. Perspectives on amyloid and Alzheimer's disease: a critical review. *Annu. Rep. Med. Chem.* 28:49–58.

Ladror, U. S., S. W. Snyder, T. F. Holzman, G. T. Wang, and G. A. Krafft. 1993. Cleavage of the amyloidogenic site of APP by cathepsin D and brain extracts. *Soc. Neurosci. Abstr.* 19:1633.

Ladror, U. S., S. W. Snyder, G. T. Wang, T. F. Holzman, and G. A. Krafft. 1994. Cleavage at the amino and carboxy termini of Alzheimer's amyloid-β by cathepsin D. *J. Biol. Chem.* 269:18422–18428.

Lansbury Jr., P. T. 1992. In pursuit of the molecular structure of amyloid plague: new technology provides unexpected and critical information. *Biochemistry.* 30:6865–6870.

LeVine III, H. 1993. Thioflavine T interaction with synthetic Alzheimer's disease beta-amyloid peptides: detection of amyloid aggregation in solution. *Protein Sci.* 2:404–410.

Masters, C. L., G. Simms, N. A. Weinman, G. Multhaup, B. L. McDonald, and K. Beyreuther. 1985. Amyloid plaque core protein in Alzheimer disease and Down syndrome. *Proc. Natl. Acad. Sci. USA.* 82:4245–4249.

Mattson, M., and R. E. Rydel. 1992. Beta-amyloid precursor protein and Alzheimer's disease: the peptide plot thickens. *Neurobiol. Aging.* 13: 617–621.

Otvos, L., G. I. Szendrei, V. M. Y. Lee, and H. H. Mantsch. 1993. Human and rodent Alzheimer beta-amyloid peptides acquire distinct conformations in membrane-mimicking solvents. *Eur. J. Biochem.* 211:249–257.

Pike, C. J., A. J. Walencewicz, C. G. Glabe, and C. W. Cotman. 1991. In vitro aging of β-amyloid protein causes peptide aggregation and neurotoxicity. *Brain Res.* 563:311–314.

Pike, C. J., D. Burdick, A. J. Walencewicz, C. G. Glabe, and C. W. Cotman. 1993. Neurodegeneration induced by beta-amyloid peptides in vitro: the role of peptide assembly state. *J. Neurosci.* 13:1676–1687.

Ponte, P., P. Gonzalez-Dewhitt, J. Schilling, J. Miller, D. Hsu, B. Greenberg, K. Davis, W. Wallace, I. Lieberburg, and F. Fuller. 1988. A new A4 amyloid mRNA contains a domain homologous to serine proteinase inhibitors. *Nature.* 331:525–527.

Selkoe, D. J. 1993. Physiological production of the β-amyloid protein and the mechanism of Alzheimer's disease. *Trends Neurosci.* 16:403–409.

Seubert, P., C. Vigo-Pelfrey, F. S. Esch, M. Lee, H. F. Dovey, D. Davis, S. Sinha, M. G. Schlossmacher, J. Whaley, C. Swindlehurst, R. McCormack, R. Wolfert, D. J. Selkoe, I. Lieberburg, and D. Schenk. 1992. Isolation and quantification of soluble Alzheimer's β-peptide from biological fluids. *Nature.* 359:325–327.

Shen, C.-L., G. L. Scott, F. Merchant, and R. M. Murphy. 1993. Light scattering analysis of fibril growth from the amino-terminal fragment of β(1–28) of β-amyloid peptide. *Biophys. J.* 65:2383–2395.

Shoji, M., T. E. Golde, J. Ghiso, T. T. Cheung, S. Estus, L. M. Shaffer, X. D. Cai, D. M. McKay, R. Tintner, B. Frangione, S. G. Younkin. 1992. Production of the Alzheimer amyloid beta protein by normal proteolytic processing. *Science.* 258:126–129.

Simmons, L. K., P. C. May, K. J. Tomaselli, R. E. Rydel, K. S. Fuson, E. F. Brigham, S. Wright, I. Lieberburg, G. W. Becker, D. N. Brems, and W. Li. 1993. Secondary structure of β amyloid peptide correlates with toxicity in vitro. *Soc. Neurosci. Abstr.* 19:397 Abstract.

Simmons, L. K., P. C. May, K. J. Tomaselli, R. E. Rydel, K. S. Fuson, E. F. Brigham, S. Wright, I. Lieberburg, G. W. Becker, D. N. Brems, and W. Y. Li. 1994. Secondary structure of amyloid β peptide correlates with neurotoxic activity in vitro. *Mol. Pharmacol.* 45:373–379.

Snyder, S. W., U. S. Ladror, G. T. Wang, G. A. Krafft, and T. F. Holzman. 1993a. Kinetics of beta-amyloid aggregate formation. *Biophys. J.* 64: A378 Abstract.

Snyder, S. W., U. S. Ladror, G. T. Wang, G. A. Krafft, and T. F. Holzman. 1993b. Hydrodynamic studies of the aggregation behavior of beta-amyloid. *Biophys. J.* 64:A378.

Snyder, S. W., U. S. Ladror, G. T. Wang, G. A. Krafft, and T. F. Holzman. 1993c. Specific inhibition of beta-amyloid 1–42 aggregation by beta-amyloid 1–40. *Soc. Neurosci. Abstr.* 19:1635.

Spencer, R. G. S., K. J. Halvserson, M. Auger, A. E. McDermott, R. G. Griffin, and P. T. Lansbury Jr. 1991. An unusual peptide conformation may precipitate amyloid formation in Alzheimer's disease: application of solid-state NMR to the determination of protein secondary structure. *Biochemistry.* 30:10382–10387.

Stafford III, W. F. 1992a. Boundary analysis in sedimentation transport experiments: a procedure for obtaining sedimentation coefficient distributions using the time derivative of the concentration profile. *Anal. Biochem.* 203:295–301.

Stafford III, W. F. 1992b. Methods for obtaining sedimentation coefficient distributions. *In* Analytical Ultracentrifugation in Biochemistry and Polymer Science. S. E. Harding, A. J. Rowe, J. C. Horton, editors. Cambridge, The Royal Society of Chemistry.

Suzuki, N., T. T. Cheung, X.-D. Cai, A. Odaka, L. Otvos Jr., C. Eckman, T. E. Golde, and S. G. Younkin. 1994. An increased percentage of long amyloid β protein secreted by familial amyloid β protein precursor (βAPP_{717}) mutants. *Science.* 264:1336–1340.

W. F. Tanzi, R. E., A. I. Mcclatchey, E. D. Lamperti, L. Villa-Komaroff, J. F. Gusella, and R. L. Neve. 1988. Protease inhibitor domain encoded by an amyloid protein precursor mRNA associated with Alzheimer's disease. *Nature.* 331:528–530.

Tomski, S. J., and R. M. Murphy. 1992. Kinetics of aggregation of synthetic beta-amyloid peptide. *Arch. Biochem. Biophys.* 294:630–638.

Turnell, W. G., and J. T. Finch. 1992. Binding of the dye Congo Red to the amyloid protein pig insulin reveals a novel homology amongst amyloid-forming peptide sequences. *J. Mol. Biol.* 227:1205–1223.

Waite, J., G. M. Cole, S. A. Frautschy, D. J. Connor, and L. J. Thal. 1992. Solvent effects on beta protein toxicity in vivo. *Neurobiol. Aging.* 13: 595–599.

Yankner, B. A. 1992. Commentary and perspective on studies of beta amyloid neurotoxicity. *Neurobiol. Aging.* 13:615–616.

Yankner, B. A., L. K. Duffy, and D. A. Kirschner. 1990. Neurotrophic and neurotoxic effects of amyloid β protein: reversal by tachykinin neuropeptides. *Science.* 250:279–282.

Zagorski, M. G., and C. J. Barrow. 1992. NMR studies of beta-peptides: proton assignments, secondary structure, and mechanism of an alpha-helix > beta-sheet conversion for a homologous, 28-residue, *N*-terminal fragment. *Biochemistry.* 31:5621–5631.